Biomedical Signal Processing and Control 33 (2017) 261–271

Contents lists available at ScienceDirect

Biomedical Signal Processing and Control

journal homepage: www.elsevier.com/locate/bspc

Towards automated electroencephalography-based Alzheimer's disease diagnosis using portable low-density devices

Raymundo Cassani[a], Tiago H. Falk[a,*], Francisco J. Fraga[b], Marco Cecchi[c], Dennis K. Moore[c], Renato Anghinah[d]

[a] Institut National de la Recherche Scientifique, Centre Énergie, Matériaux, Télécommunications, University of Quebec, Montreal, QC, Canada
[b] Engineering, Modelling and Applied Social Sciences Center, Universidade Federal do ABC, São Paulo, Brazil
[c] Neuronetrix, Louisville, KY, USA
[d] Reference Center of Behavioural Disturbances and Dementia, School of Medicine, Universidade de São Paulo, São Paulo, Brazil

ARTICLE INFO

Article history:
Received 23 August 2016
Received in revised form
11 November 2016
Accepted 12 December 2016
Available online 21 December 2016

Keywords:
Alzheimer's disease (AD)
Electroencephalography (EEG)
Portable
Low-density
Amplitude modulation
Spectral power
Coherence
Diagnosis

ABSTRACT

Today, Alzheimer's disease (AD) diagnosis is carried out using subjective mental status examinations assisted in research by scarce and expensive neuroimaging scans and invasive laboratory tests; all of which render the diagnosis time-consuming, geographically confined and costly. Driven by these limitations, quantitative analysis of electroencephalography (EEG) has been proposed as a non-invasive and more convenient technique to study AD. Published works on EEG-based AD diagnosis typically share two main characteristics: EEG is manually selected by experienced clinicians to discard artefacts that affect AD diagnosis, and reliance on EEG devices with 20 or more electrodes. Recent work, however, has suggested promising results by using automated artefact removal (AAR) algorithms combined with medium-density EEG setups. Over the last couple of years, however, low-density, portable EEG devices have emerged, thus opening the doors for low-cost AD diagnosis in low-income countries and remote regions, such as the Canadian Arctic. Unfortunately, the performance of automated diagnostic solutions based on low-density portable devices is still unknown. The work presented here aims to fill this gap. We propose an automated EEG-based AD diagnosis system based on AAR and a low-density (7-channel) EEG setup. EEG data was acquired during resting-awake protocol from control and AD participants. After AAR, common EEG features, spectral power and coherence, are computed along with the recently proposed amplitude-modulation features. The obtained features are used for training and testing of the proposed diagnosis system. We report and discuss the results obtained with such system and compare the obtained performance with results published in the literature using higher-density EEG layouts.

1. Introduction

The term dementia is used to encompass a number of neurodegenerative diseases and conditions that have their origin in damage and death of neurons. Among the different diseases classified as dementia, Alzheimer's disease (AD) is the most frequent, accounting for 60–80% of dementia cases worldwide. AD is a chronic neurodegenerative disorder that causes decay in the number of synapses and eventual death of neurons. This process may begin 20 or more years before behavioural symptoms appear. At early stages of AD, these brain changes do not affect individual's life style. The progression of AD leads to a decline and, consequentially, loss of both cognitive (e.g., memory, reasoning, communication) and behavioural functions that interfere with the individual's daily life. In the final stages of the disease, the individual requires round-the-clock care. AD is ultimately fatal [1,2].

Studies show that in 2013 44.4 million people were suffering from dementia worldwide, and this number is projected to grow to 75.6 million by 2030 and to 135.6 million by 2050. Because of the increased life expectancy around the world, most of the dementia cases (approximately 70%) will take place in low- and middle-income countries, as depicted in Fig. 1. AD not only affects individuals but also their families whom become caregivers as the pathology progress. Moreover, the economic impact of dementia represents a great toll on society. For example, in 2010 the global annual cost for dementia care was estimated at US$604 billion, i.e.

* Corresponding author.
E-mail addresses: raymundo.cassani@gmail.com (R. Cassani), falk@emt.inrs.ca (T.H. Falk), franciscojfraga@gmail.com (F.J. Fraga), mcecchi@neuronetrix.com (M. Cecchi), dmoore@neuronetrix.com (D.K. Moore), anghinah@terra.com.br (R. Anghinah).

http://dx.doi.org/10.1016/j.bspc.2016.12.009
1746-8094/

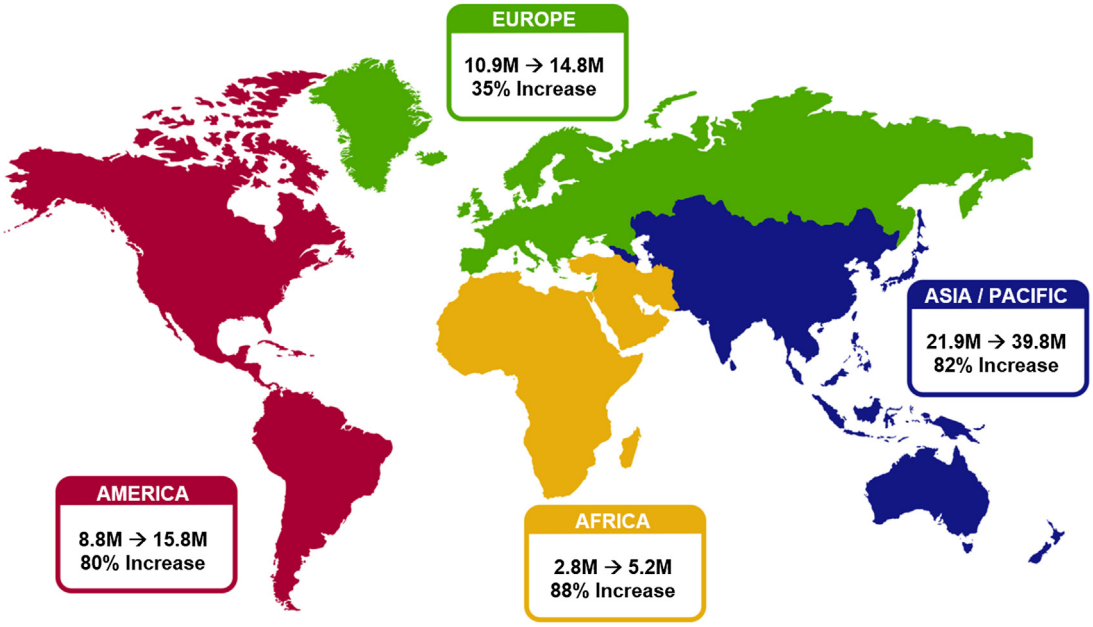

Fig. 1. Global dementia incidence in 2013 and projected increase by 2030.

twice the Exxon Mobil revenue for the same year, and it is expected to increase by 85% by the year 2030 [2,3].

Due to the serious implications of current and future global number of dementia cases, the World Health Organization has made an urgent call to include dementia in the public health agenda of each country, with the objective of improving (early) diagnosis and providing better care and support for patients, their families, and caregivers [1].

Despite the fact that today there are no treatments to cure or alter the progression of AD, an accurate and early diagnosis empowers AD patients and their families to learn about the disease, look for palliative therapies, deal with financial and legal decisions, carry out housing and healthcare arrangements, look for support community groups, and actively promote AD awareness and research [2]. Moreover, novel disease-modifying drugs are being studied and developed around the world, and it is likely that their efficacy will be higher in early stages of AD [4], thus making early diagnosis a pivotal element in AD research and therapy.

Nowadays, AD diagnosis is performed following the criteria of the Diagnostic and Statistical Manual of Mental Disorders, either fourth edition (DSM-IV-TR) or fifth edition (DSM-5), the National Institute of Neurological Disorders and Stroke and Alzheimer Disease and Related Disorders (NINCDS–ADRDA) Work Group, and neurophysiological tests as the Mini-Mental State Evaluation (MMSE) [5]. In research, these criteria are commonly assisted by biomarkers obtained through structural neuroimaging with magnetic resonance imaging (MRI) and/or molecular neuroimaging with positron emission tomography (PET), by methods that aim at finding tissue damage in specific structures of the brain, and/or by cerebrospinal fluid analysis with the objective of finding AD-related compounds.

AD diagnosis based on the former criteria leads to accuracies ranging from 85 to 95%, and relies on experienced clinicians, meticulous and exhaustive testing sessions, as well as costly and scarce neuroimaging tools and invasive procedures [6]. Unfortunately, definite AD diagnosis is only confirmed through post-mortem examination of brain tissue. These constraints limit the implementation of early AD diagnosis in low-income countries, remote and rural regions, as well as in metropolitan areas where wait times for non-emergency MRIs can be in the order of months [7], thus making quantitative electroencephalography (qEEG, henceforth referred to as EEG) a promising tool for Alzheimer's disease diagnosis.

Over the last few decades, quantitative electroencephalography has been successfully utilized as a reliable technology for the study and diagnosis of cortical disorders. EEG signals consist of recordings of changes in the electric potential measured at the scalp; these changes have their origin in the electrical activity evoked by the neurons synchronized firing in the cerebral cortex. Therefore, the EEG signal provides a global snapshot of the underlying brain activity. The commonly used "international 10-20 system" electrode layout, is depicted in Fig. 2a, and the acquired EEG signals are presented in Fig. 2b. For analysis, EEG signals are generally divided into 5 major frequency bands, namely: delta (δ) 0.1–4 Hz, theta (θ) 4–8 Hz, alpha (α) 8–12 Hz, beta (β) 12–30 Hz and gamma (γ) >30 Hz [8]. Fig. 2c shows an EEG signal from one electrode decomposed into its major component bands. It is common to represent the EEG signals and their major bands in the frequency domain, as depicted by Fig. 2d. Unlike other biopotentials (such as the electrocardiographic signals), EEG signals are rarely analysed by the naked eye, thus further processing is required to identify patterns and extract valuable information form EEG recordings.

EEG represents a non-invasive and inexpensive technique for the study of neurodegenerative disorders. Thus, it has emerged as an interesting tool for the study and diagnosis of AD. While traditional EEG devices are expensive and hard to transport, advances in the manufacturing of electronic devices have led to the recent appearance of affordable portable wireless EEG devices, opening the doors to EEG-based AD diagnosis in developing countries and geographically remote regions.

The ultimate aim of this paper is to propose and discuss the development and performance of an automated EEG-based AD diagnosis system relying in portable EEG devices. In order to achieve this goal, the next section will present relevant aspects of EEG-based AD diagnosis, placing emphasis on the existing challenges that arise with the use of portables EEG devices.

2. EEG-based AD diagnosis

Since EEG signals reflect functional changes in the cerebral cortex, they can be used to infer neuronal degeneration and decay

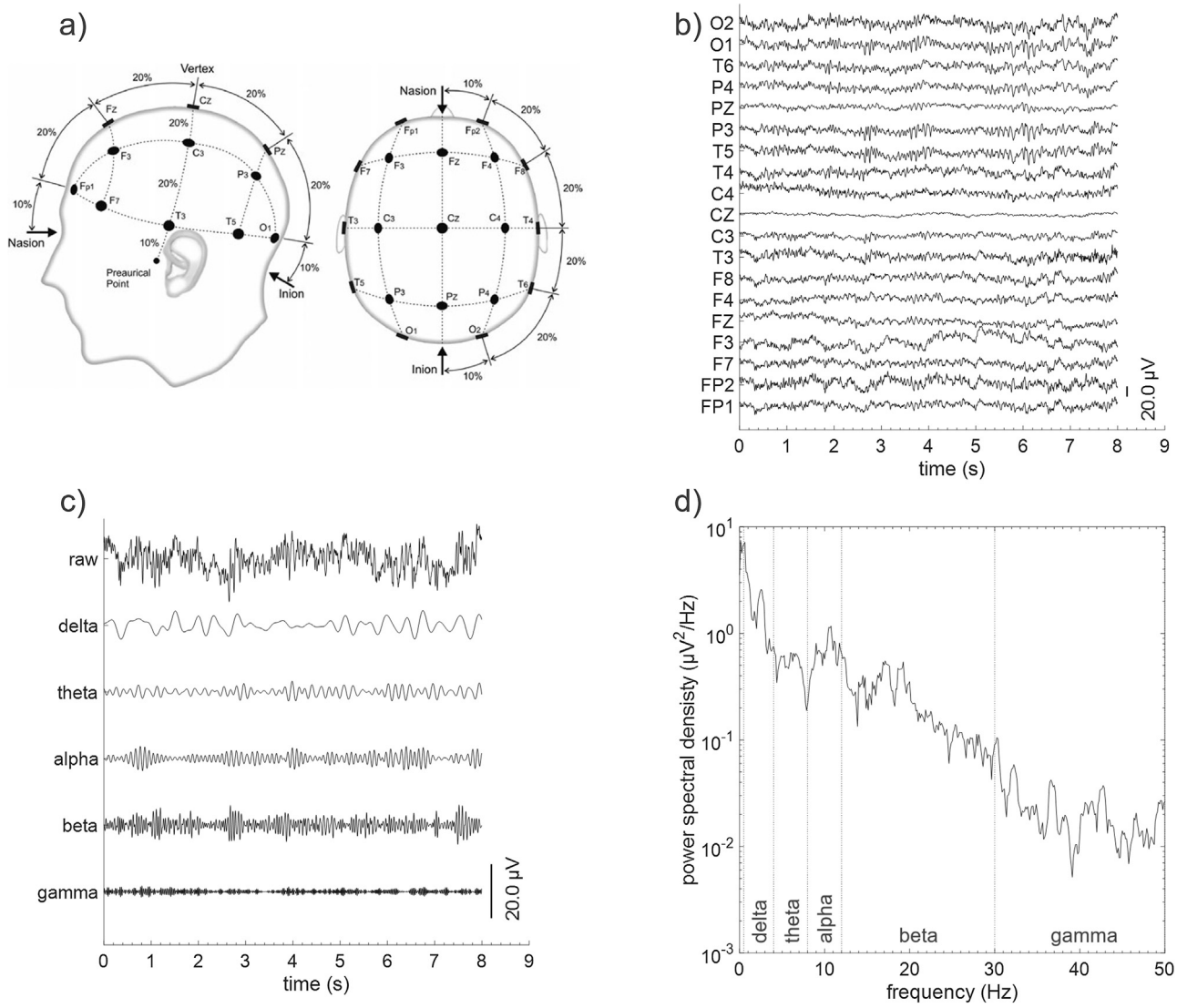

Fig. 2. (a) EEG electrodes in the international 10-20 system layout. (b) EEG signals in time domain from different electrodes. (c) Decomposition of a one-electrode (C3) EEG signal into major bands. (d) Spectral representation of EEG bands for EEG signal at electrode C3.

in the number of synapses, thus functional impairment caused by the progression of AD long before actual tissue loss or behavioural symptoms appear. Several studies have explored the EEG abnormalities related to AD. Typically, four major effects of AD on the EEG signals have been repeatedly observed:

i Slowing of EEG signal. Detected as differences in the power distribution among frequency bands between healthy aging and AD patients, it is characterized by a shift of the EEG power spectrum from high frequencies (alpha and beta) to lower frequencies (delta and theta). The degree of the shift correlates with AD severity. The slowing of the EEG signals is thought to have its origin in the loss of cholinergic innervations observed in AD patients [9–11]

ii Reduced complexity. Globally decreased complexity of brain electrical activity in AD patients, likely caused by reduced connections between cortical regions and/or neuronal death that lead to lower interaction of neuronal networks, leading to simpler (less complex) EEG dynamics. Reduction of EEG complexity during AD usually is evaluated via nonlinear dynamical analysis [9,10]

iii Decreased synchrony. A decrease in synchronization has been associated with AD patients. While the biophysical mechanisms for reduced synchrony in AD are not well understood, one hypothesis suggests its origins in the atrophic communication in the neuronal networks. Reduced spectral coherence among cortical regions, specifically between left and right hemispheres, has been reported in AD [12,13]

iv Neuromodulatory deficit in EEG rhythms. Recent experimental evidence has suggested a neuromodulatory deficit in AD [14,15]. To quantify the neuromodulatory activity, amplitude modulation analysis has been proposed as a spectro-temporal technique that allows direct characterization of cross-frequency interaction effects by measuring rates at which EEG bands are modulated [16,17]

For the quantitative evaluation of the effects of AD in the EEG signal, diverse signal processing techniques have been proposed in the literature. Table 1 lists these techniques together with the major effects of AD on EEG that are quantified. Combined, these different signal processing techniques have been shown to achieve between 80 and 90% AD diagnostic accuracy, in line with alternate, more expensive neuroimaging tools [18,19]. A full description of these

Table 1
Major effects of AD over EEG signal and signal processing techniques to measure those effects. More details about the listed features can be found in [10].

Major effect	Signal processing Techniques	
Slowing	Spectral power	
	Spectrogram	
	Wavelet analysis	
Reduced complexity	Entropy measures	Fractal dimension
	Auto-mutual information	Lyapunov exponent
	Lempel-Ziv complexity	
Decreased synchrony	Pearson correlation coefficient	Granger causality
	Magnitude coherence	Phase synchrony
	Phase coherence	Global Field Synchrony
	Mutual Information	Cross-frequency coupling
Neuromodulatory deficit	Hilbert transform	
	Amplitude modulation analysis	

techniques is beyond the scope of this work, but the interested reader is referred to Refs. [9–13,15–18] for more complete details.

2.1. EEG recording conditions

Most published studies on EEG-based AD diagnosis have consistently acquired EEG signals during resting-awake (either eyes-open or eyes-closed) experimental protocols. The motivation for these protocols lies in the reduction of noise related to artefacts (undesired signals which corrupt EEG signal) from the acquired signals, allowing longer-duration and cleaner signals for analysis. Resting-awake EEG analyses, however, assess only the differences in resting default mode networks between healthy controls and AD patients, thus reaching an accuracy between 80 and 90%, which is further reduced to 70% if multiple stages of AD are considered [17].

Neuropathological evidence suggests that AD-related atrophy may begin in the entorhinal cortex and subsequently spread to its connected brain regions such as the mediotemporal structures [20]. As such, it has been proposed that EEG signals recorded during different experimental protocols will lead to greater discriminatory power between healthy controls and AD patients of varying levels. These experimental protocols include those with the presence of visual, auditory [21], or olfactory stimuli [22], as well as those with the presence of specific cognitive tasks, such as an oddball paradigm [23,24], visual memory [25], or working memory [26].

2.2. Common EEG artefacts

One of the major shortcomings of AD diagnosis using EEG is that it is inherently susceptible to artefacts, such as eye movements and blinks, heartbeats, cranial muscle activity, electrode displacements caused by head movements and power line interference, all of which have detrimental effects on the signal to noise ratio of the EEG data. As such, if proper care is not taken, overall AD diagnosis performance may be significantly compromised. To overcome this shortcoming, most studies have relied on: (1) acquiring EEG signals during resting-state experimental protocols, and (2) using artefact-free EEG segments (called epochs) which are selected by expert clinicians via meticulous visual inspection [11–16,27]. Unfortunately, such dependence on human selection of artefact-free epochs has several disadvantages, including (1) the introduction of human biases and errors that can make the results irreproducible, (2) making the diagnostic task tedious, time consuming and expensive, as well as (3) removing diagnostic information from e.g., frontal electrodes which tend to be severely contaminated by eye blinks and movements [28].

As an alternative to manual selection of clean EEG signals, artefact removal algorithms have been proposed [29]. These algorithms are classified as either “semi-automated” or “automated”, depending on the need for human intervention. Methods based on independent component analysis (ICA) can be regarded as semi-automated as human assessment is often required to differentiate between artefactual and EEG signal components [30]. On the other hand, methods such as statistical artefact rejection [31], adaptive noise cancelling [32], wavelet enhanced ICA [33], multivariate singular spectrum analysis [28], and feature averaging [34], are examples of automated artefact removal (AAR) algorithms which do not require human intervention.

Recent studies have explored the effects of artefact removal algorithms on AD diagnosis; in [35] the effects of semi-automated algorithms based on blind source separation paradigms were explored. Moreover, a comparison of the effects of different automated artefact removal algorithms on EEG-based AD diagnosis was presented in Ref. [19] for different EEG features.

2.3. Portable devices

Over the last few years, the miniaturization of EEG equipment has led to the proliferation of portable wireless headsets. Such headsets have several interesting advantages compared with their research-grade counterparts, such as: (1) reduced hardware-related stress to the user during headset preparation and during recordings, thus reducing distractions and allowing longer recordings in more natural positions or activities, such as book reading or TV watching, (2) since wires are eliminated, transportation of these devices is facilitated, and given their ubiquitous data transmission protocols (e.g., Bluetooth or Zigbee), recording and processing of EEG signals on mobile devices has become a reality, and lastly, (3) the lower power consumption requirements have allowed for long-term recordings while subjects are performing their daily activities, thus making ambulatory EEG practical. A review on portable EEG devices is presented in Refs. [36,37].

Published works on EEG-based AD diagnosis have typically relied on EEG setups ranging from 16, 20, 32, 64, or 128 electrodes [11–16,27]. Such systems are cumbersome and time consuming to place on the participants, sometimes taking up to one hour only for the EEG headgear preparation. This can have serious outcomes for AD diagnosis, as drowsiness, fatigue, stress, and/or alternate mental states may alter EEG patterns, thus deteriorating diagnostic accuracy. Moreover, such medical-grade systems are hard to transport and expensive to fund in low- and middle-income countries, as well as in remote and rural regions of developed countries. As such, it is important that we explore the benefits of using low-density portable systems for AD diagnostic purposes. The next section presents the implementation of the abovementioned methods for automated EEG-based AD diagnosis based on a commercial low-density EEG setup comprised of 7 electrodes.

3. Material and methods

In Fig. 3, the main stages of the proposed automated EEG-based AD diagnosis system are depicted, namely: Pre-processing and AAR

Table 2
Demographics for Neuronetrix AD dataset.

Cohort	Group Identifier	Subjects (female)	Age [years]	Education [years]
AD participants	AD	99 (50)	76.3 ± 7.4	14.2 ± 3.1
Control participants	N	85 (49)	72.9 ± 7.3	14.9 ± 3.0

Table 3
Demographics for Brazil AD dataset.

Cohort	Group Identifier	Subjects (female)	Age [years]	Education [years]
AD participants	AD	35 (20)	74.9 ± 8.9	5.2 ± 3.1
Control participants	N	24 (12)	66.3 ± 8.8	10 ± 3.4

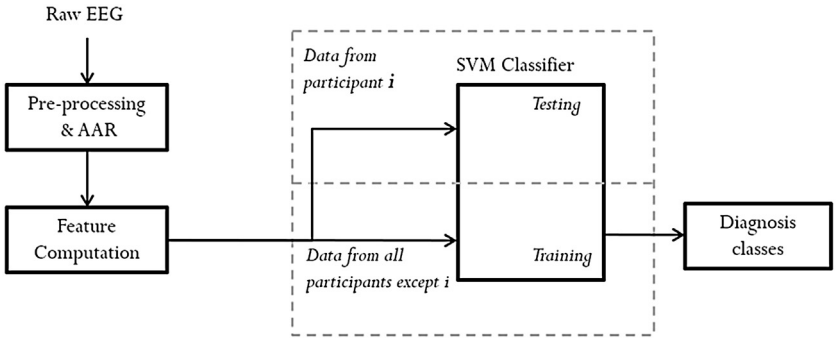

Fig. 3. Block diagram of an EEG-based AD diagnosis system, indicating its main stages.

algorithms (Section 3.3), Feature Computation (Section 3.4) and Classification and Diagnosis Classes (Section 3.5).

3.1. Participants

Recently, Neuronetrix, a US-based company, recruited participants over a 2-year clinical study across major Alzheimer's Disease Centres in the US [38]. Participants were divided into those suffering AD and healthy aging subjects. The first group (AD) consisted of 99 participants who were diagnosed according to the NINCSD-ADRDA and DSM-IV criteria, and had an MMSE score between 21 and 26. The second group (N) was comprised by 85 healthy subjects matched for age and gender, with an MMSE score ≥27. Table 2 presents the demographics for the participants used in this study.

In another AD study, fifty-nine participants were recruited by the Behavioural and Cognitive Neurology Unit of the Department of Neurology and the Reference Centre for Cognitive Disorders at the Hospital das Clinicas in São Paulo, Brazil. AD patients were diagnosed by experienced neurologists according to NINCDS-ADRDA criteria and classified based on the Brazilian version of the MMSE. Participants were divided into two groups. The AD group comprised 35 mild-to-severe AD patients, MMSE score <24 and a Clinical Dementia Rating (CDR) between 0.5 and 2. Inclusion criteria for the N group included an MMSE score ≥25, and CDR = 0. Table 3 presents the demographics for this second study cohort.

In both studies, additional criteria for inclusion in the AD group, were the presence of functional and cognitive decline over the previous 12 months based on detailed interviews with knowledgeable informants, and absence of diabetes mellitus, kidney disease, thyroid disease, alcoholism, liver disease, lung disease or vitamin B12 deficiency, as these conditions can also cause cognitive decline.

3.2. Data acquisition and apparatus

EEG data for the Neuronetrix AD study were collected during a 3-min resting-awake eyes-open period. The Neuronetrix proprietary 7-channel COGNISION^{TM} device (Fig. 4a) was used for data collection. The device uses a sampling frequency of 125 Hz and biauricular referential electrodes [24]. The electrode layout is presented in Fig. 4b. Data from this study is referred henceforth as the 'Neuronetrix' dataset.

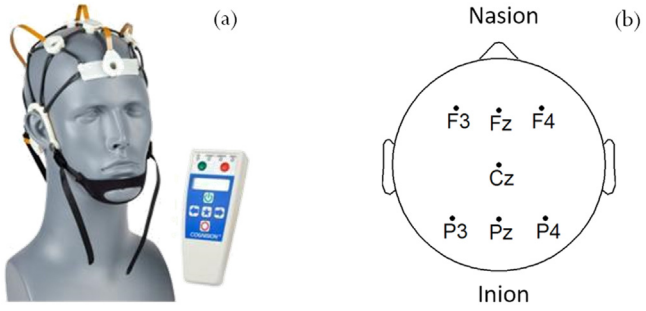

Fig. 4. Neuronetrix proprietary COGNISION^{TM} system. (b) EEG electrode placement for the Neuronetrix study.

EEG data from the Brazilian AD study (henceforth referred as the 'Brazil' dataset), were acquired using a resting-awake eyes-closed paradigm for 8 min. The Braintech 3.0 EEG device (EMSA Equipamentos Médicos Inc., Brazil) was used for data collection, with a 200 Hz sample frequency and 20 scalp electrodes placed according to the international 10-20 layout system. Biauricular referential electrodes were attached, as recommended by the Brazilian Society of Clinical Neurophysiology and the American Clinical Neurophysiology Society [39]. In order to compare results, the Brazil dataset was decimated channel-wise to have the same electrode layout as in the Neuronetrix dataset (Fig. 4b).

3.3. Pre-processing of EEG signal

To facilitate comparisons, the pre-processing pipeline for both datasets was identical. A zero-phase finite impulse response (FIR) band-pass filter with a bandwidth 0.5–45 Hz was utilized. Motivated by our recent findings on detrimental effects of artefacts in AD

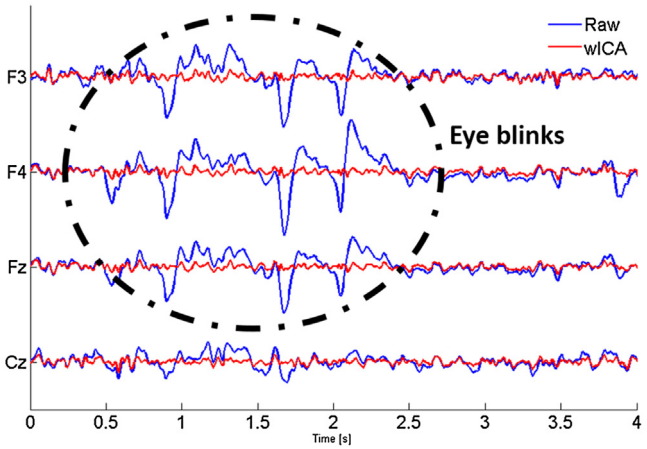

Fig. 5. Plots of raw (blue) and wICA-processed (red) EEG signals for four of the collected 7 electrodes, namely F3, F4, Fz and Cz. (For interpretation of the references to colour in this figure legend, the reader is referred to the web version of this article.)

diagnosis [19], we used the wavelet-enhanced independent component analysis (wICA) algorithm. The wICA algorithm decomposes the EEG signals into independent components (IC), then a wavelet transform is applied to each IC, and their respective wavelet coefficients undergo a thresholding process to differentiate between neural and artefactual coefficients. The inverse wavelet transform is then used to recover the artefact-cleaned IC, which, in turn, are used to reconstruct the artefact-free EEG signals. The parameter used for the wICA algorithm was a threshold K = 1.0 [33]. For illustration purposes, Fig. 5 presents a representative EEG segment before (blue) and after wICA processing (red).

To assess the effects of AD on the collected EEG signals, common EEG features utilized in AD diagnosis were used, as detailed below.

3.4. Feature computation

As shown in Fig. 3, the next stage in the automated AD diagnosis system after artefact removal is feature computation. This step has the objective of quantifying the effects of AD on the EEG signals. In this work, features were computed over windows (also called epochs) with a length of 8 s and 1-s shifts between consecutive epochs. Previously-proposed feature classes shown to reliably characterize AD are explored, namely: spectral, coherence, and amplitude modulation features.

3.4.1. Spectral power features

As their name suggests, spectral power features measure the power present in well-defined EEG frequency bands. The spectral features computed during our experiments were: delta (0.1–4 Hz), theta (4–8 Hz), alpha (8–12 Hz), low-alpha (8–10 Hz), high-alpha (10–12 Hz), beta (12–30 Hz), delta-to-beta (0.5–30 Hz), theta-to-beta (4–30 Hz) and low-gamma (30–45 Hz). To calculate the power of each of these nine bands, the full-band EEG signal from one electrode is frequency-decomposed into the time series of each frequency band by using the corresponding zero-phase FIR bandpass filter (similar to Fig. 2c). Then the power for a certain frequency band in a given epoch with m samples is computed as Eq. (1), where x(k) represents the time series for a frequency band in one electrode.

$$power = \frac{1}{m}\sum_{k=1}^{m} x^2(k) \tag{1}$$

The power for each individual band is then normalized by the full band EEG power. Thus, for this analysis a total of 63 (9 frequency bands × 7 electrodes) spectral power features were thus computed per each epoch.

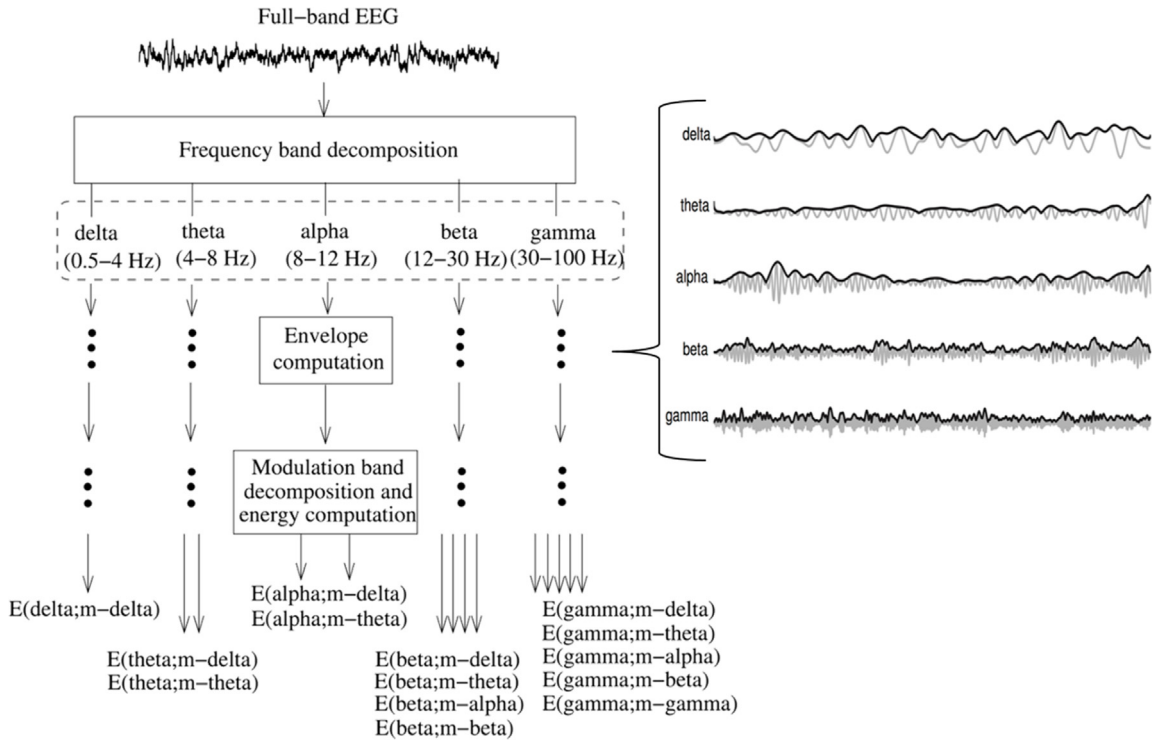

Fig. 6. Algorithm used to compute Amplitude Modulation Features Subplots on the right illustrate the five frequency bands (grey) and their respective Hilbert temporal envelopes (black).

3.4.2. Coherence features

Coherence features have been used as indicators of cortical connectivity, as they measure the co-variance between either two power spectra (termed magnitude square coherence, MSC) or two phase signals (phase coherence) [40]. Coherence features were computed for delta, theta, alpha, beta and gamma bands for 5 pairs of electrodes, namely: Fz -Pz, F3 -F4, P3 -P4, F3 - P3 and F4 - P4.

The analytic signal for each of the EEG component bands was computed using the Hilbert transform, then the auto-spectrum and cross-spectrum were computed by Eqs. (2) and (3) respectively,

$$P_{xx} = \frac{1}{m}\sum_{k=1}^{m} x(k)\bar{x}(k) \tag{2}$$

$$P_{xy} = \frac{1}{m}\sum_{k=1}^{m} x(k)\bar{y}(k) \tag{3}$$

where x(k) and y(k) are the analytic signals in an epoch for a given frequency band in the two electrodes of a pair, and $\bar{x}$(k) and $\bar{y}$(k) are their respective conjugated. Then the MSC and phase coherence are defined in Eqs. (4) and (5), respectively.

$$MSC = \frac{|P_{xy}|^2}{P_{xx}P_{yy}} \tag{4}$$

$$PhaseCoherence = \arg\left(P_{xy}\right) \tag{5}$$

In total 25 (5 bands × 5 pairs) MSC and 25 phase coherence features were computed per epoch.

3.4.3. Amplitude modulation features

EEG amplitude modulation features have been recently proposed and shown to be useful for AD detection and monitoring disease progression [17]. These features characterize the modulation relationship between the different EEG bands for a given electrode, i.e., they characterize the amplitude-amplitude cross-frequency coupling of EEG signals [16]. As shown in Fig. 6, three steps are required in order to compute amplitude modulation features. First, the full-band EEG is frequency-decomposed into the five principal frequency bands (delta, theta, alpha, beta and gamma) by zero-phase FIR filters. Then, the analytic signal for each frequency band is computed using the Hilbert transform, and from its magnitude is used to obtain the amplitude modulations of each band. Lastly, to characterize the cross-frequency dynamics of the amplitude modulations, a second frequency decomposition is performed on the band envelope signals, this decomposition is designed to coincide with the frequency ranges of the five frequency bands. To distinguish between frequency and modulating bands time series, the latter are referred to in here as m-delta, m-theta, m-alpha, m-beta and m-gamma. The power of the band-mband time series was computed using (1) and normalized by the full band EEG power.

It is important to emphasize that, due to properties of the Hilbert transform (e.g., Bedrosian's theorem), not all frequency-modulation band combinations make sense [16]. Henceforth, the notation frequency band – modulating band is used to denote the normalized power for a given frequency and modulating band. Only the following frequency-modulation band combinations are relevant: delta-mdelta, theta-mdelta, -mtheta; alpha-mdelta, -mtheta; beta-mdelta, -mtheta, -malpha, -mbeta; and gamma-mdelta, -mtheta, -malpha, -mbeta, -mgamma [19]. As such, these 14 features were computed for each of the 7 EEG signals, thus totalling 126 amplitude modulation features per epoch.

Overall, a total of 211 (spectral, coherence and amplitude modulation) features were computed for each 8-s epoch available in the two available datasets, as summarized in Table 4.

Table 4
Features computed for each 8-s epoch.

Feature Group	Features
Spectral (computed per electrode)	delta
	theta
	alpha
	low alpha
	high alpha
	beta
	delta to beta
	theta to beta
	low-gamma
Coherence (computed per electrode pair)	MSC delta
	MSC: theta
	MSC: alpha
	MSC: beta
	MSC: gamma
	Phase coherence delta
	Phase coherence theta
	Phase coherence alpha
	Phase coherence beta
	Phase coherence gamma
Amplitude Modulation (computed per electrode)	delta – mdelta
	theta – mdelta
	theta – mtheta
	alpha – mdelta
	alpha – mtheta
	beta – mdelta
	beta – mtheta
	beta – malpha
	beta – mbeta
	gamma –mdelta
	gamma – mtheta
	gamma –malpha
	gamma – mbeta
	gamma –mgamma

3.5. Classification and statistical analysis

The Support Vector Machine (SVM) algorithm has been widely used as classifier in AD [16,41]. The principle behind the SVM algorithm is to map data points into a higher dimension in which the data points can be separable by a hyperplane. A complete description of the SVM algorithm is beyond the scope of this work and the interested reader is referred to [42,43] from more complete details. A SVM classifier was utilized for classification in both datasets, Neuronetrix and Brazil. together with the L1-norm as penalization, as this presents advantages with respect to the traditional L2-norm, more specific, the use of L1-norm leads to sparse weight vectors, thus feature selection and classification are accomplished in the same step [44]. In our experiments, the open-source scikit-learn (machine learning for Python) [45] SVM implementation was used, with the following parameters: linear kernel, L1-norm penalization, and a default regularization coefficient value of C = 1.

In order to evaluate the classifier performance, we made use of two different cross-validation (CV) approaches (for both datasets): 10-fold and Leave-One-Subject-Out. The 10-fold CV is commonly used to report classifier performance. In 10-fold CV, data is randomly divided in ten partitions, then nine are used for classifier training and one partition for testing, this process is repeated 10 times, and the accuracy is calculated combining the label outputs from all the testing partitions, i.e., sample-wise. In LOSO CV, in a dataset with N participants, data from N-1 subjects is used for classifier training while data from the remaining subject is used for testing, this CV approach is depicted in Fig. 3. To evaluate the classifier performance under LOSO CV, each participant is labelled as control (N) or AD based on majority vote, i.e., if 50% or more of the participant's epochs belong to a given class the participant is assigned to that class. Then, performance is calculated subject-wise. The reason behind using LOSO CV, is to avoid the optimistic bias

Table 5
Classification performance comparison of the proposed system in Neuronetrix and Brazil dataset.

System	Accuracy (%)	Sensitivity (%)	Specificity (%)
Benchmark LOSO	81.4	75.0	85.7
Neuronetrix LOSO CV	63.1	68.7	56.5
Brazil LOSO CV	69.5	71.4	66.6
Neuronetrix 10-fold CV	77.3	79.2	75.2
Brazil 10-fold	91.4	92.9	89.2

present in 10-fold CV, which is introduced by the random division of data in partitions; refer to 'Cross-validation approaches' in the Discussion Section. For comparison purposes, we use as Benchmark the reported classification performance published in [46] which were obtained with the full Brazil dataset, i.e., data from all 20 electrodes and LOSO CV approach.

Lastly, to test if the features exhibited a statistically significant difference between the AD and control groups, a Kruskal-Wallis test with Dunn-Sidak post-hoc correction was used [47]. Statistical significance was established at a 1% level.

4. Results

Table 5 summarises the classification performance (accuracy, sensitivity, and specificity) for the Benchmark (system using the full Brazil dataset, i.e., EEG data from 20 electrodes, and LOSO CV), and the different combinations of 7-channel datasets: Neuronetrix (resting-state eyes-open) and Brazil (resting-state eyes-closed), using two CV approaches: 10-fold and LOSO. A detailed analysis of the results presented in Table 5 is provided in the Discussion Section.

Taking into consideration only the top-35 features for each dataset, Table 6 lists such features as well as highlights which are common between the two datasets. Features which exhibited a significant difference ($p < 0.01$) between the control and AD groups are followed by an asterisk in the Table. For common features in both datasets, symbols ↑ and ↓ indicate whether the median of the respective feature was higher or lower in the AD cohort, respectively.

Table 6
List of top-35 features from the systems. Features in gray background are present in both columns. Features followed by an * presented significant differences between control and AD cohorts; statistical Kruskal-Wallis test ($p < 0.01$) with Dunn-Sidak post-correction. For common features in both datasets, symbols ↑ and ↓ indicate whether the median of the respective feature was higher or lower in the AD cohort, respectively.

Ranking	Neuronetrix	Brazil
1	alpha_Cz * ↓	alpha_Cz * ↓
2	tab_Cz *	beta_Pz * ↓
3	alpha_Fz * ↓	theta_Pz * ↑
4	msc_beta_Fz_Pz *	delta_Pz *
5	beta_Pz * ↓	gamma_F3 * ↓
6	gamma_Pz * ↑	gamma_P4 * ↓
7	beta_Cz *	dtab_P3 * ↑
8	tab_Fz	alpha_P4 *
9	alpha1_P3 *	beta_P4 *
10	alpha_Pz	alpha1_Cz * ↑
11	alpha2_P3	delta_P3 *
12	tab_Pz *	beta_P3 * ↓
13	alpha_P3 *	alpha_Fz * ↓
14	alpha1_Pz	gamma_Pz ↓
15	theta_F4 *	gamma_P3 * ↓
16	gamma_P3 ↑	alpha2_Cz *
17	alpha2_Fz * ↓	msc_gamma_P3_P4 *
18	msc_beta_F4_P4 ↓	alpha1_P4 *
19	gamma_F3 ↓	theta_P3 *
20	msc_theta_P3_P4 * ↓	beta_F3 * ↓
21	alpha1_F3 *	dtab_P4 *
22	delta_Cz *	beta_F4 *
23	gamma_Fz	dtab_Cz *
24	dtab_Fz	alpha2_Pz * ↓
25	dtab_P3 ↓	delta_P4 * ↑
26	beta_P3 * ↓	theta_Fz *
27	alpha2_Pz ↓	msc_beta_F4_P4 * ↓
28	beta_F3 * ↓	gamma-malpha_F4
29	alpha1_Cz * ↓	msc_theta_P3_P4 * ↓
30	theta_Pz * ↑	msc_alpha_P3_P4 *
31	gamma_P4 ↑	beta-malpha_Cz *
32	delta_P4 * ↑	beta-malpha_Fz *
33	delta_F4 *	msc_theta_Fz_Pz *
34	msc_gamma_Fz_Pz *	alpha1_Fz *
35	delta_Fz	alpha2_Fz * ↓

5. Discussion

5.1. Cross-validation approaches

Classification performance was higher when using 10-fold CV than when using LOSO CV (Table 5). This is due to the fact that 10-fold CV introduces an optimistic bias in the estimation of the classifier performance, because of the random selection of the data partitions, data samples from the same subject are found in the training and testing data partitions for the same classifier model, as consequence, the classifier is trained and tested in data that is highly correlated and is not evaluated on true unseen data. In order to avoid that bias, we evaluate the proposed system by using the LOSO as CV. Under this CV approach, the classifier is trained with all data available but one subject, thus the performance is evaluated in never-seen data, which gives a good idea of generalization of the model.

5.2. Overall performance

From Table 5 it can be appreciated that diminishing the number of electrodes, from 20 in the Benchmark system to 7 in the proposed system (i.e. Brazil LOSO) led to a decrease in AD diagnosis performance in the Brazil dataset. In general, the performance of the Benchmark (20 electrodes) is considerably higher than the low-density setups, this could be attributed to the fact that a higher density layout presents a broader spatial distribution on the scalp, thus it can register cortical activity from other areas such as temporal and occipital lobes. In addition, a higher density coverage may be able to pick up spatially broad activities caused by deep brain structures, which are the first-affected by AD progression.

Moreover, the somewhat higher results obtained on the Brazil dataset may be due to the fact that the AD and N groups were not education, gender or age-balanced, as in the Neuronetrix dataset. Such factors have been shown to be important in AD progression [2]. Another plausible cause for the performance difference between datasets is the quantity of available data per each participant, 8 min for Brazil dataset and 3 min for Neuronetrix dataset.

5.3. Top-35 features and common features

An in-depth analysis of the top-selected features, Table 6, shows that almost 50% (17 over 35) of these features are common for Neuronetrix and Brazil datasets. In both datasets, it can be noted that AD cohort presents decreased medians for power features corresponding to alpha and beta bands and increased medians for power features in delta and theta bands when compared with control cohort. This shift in the power spectrum from high frequencies to low frequencies during AD is congruent with the slowing effects of AD in the EEG signals previously reported in the literature [9–11]. Nevertheless, in [48] it is reported an increment in gamma band power for the AD cohort, while in [49] and [50] the opposite effect is observed. Such contradictory findings may have origin in the EEG recording conditions, which consisted in resting-awake eyes-open

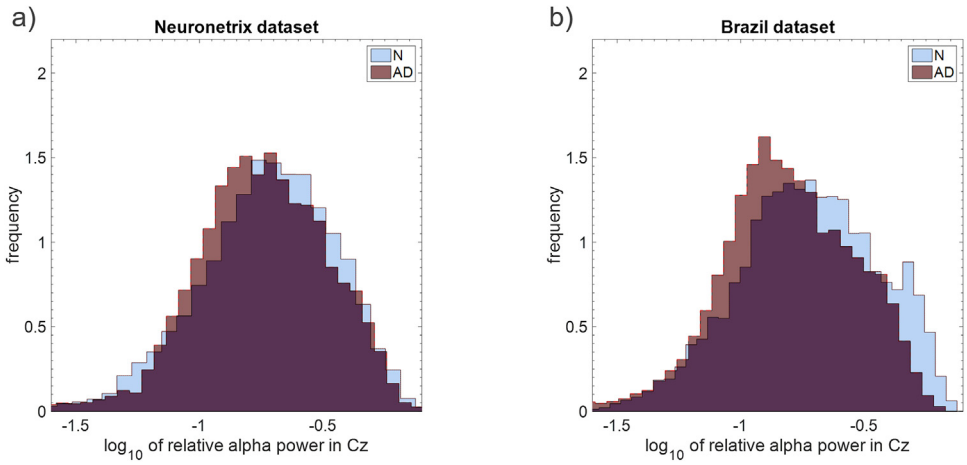

Fig. 7. Histograms for alpha relative power in electrode Cz. (a) Neuronetrix and (b) Brazil dataset.

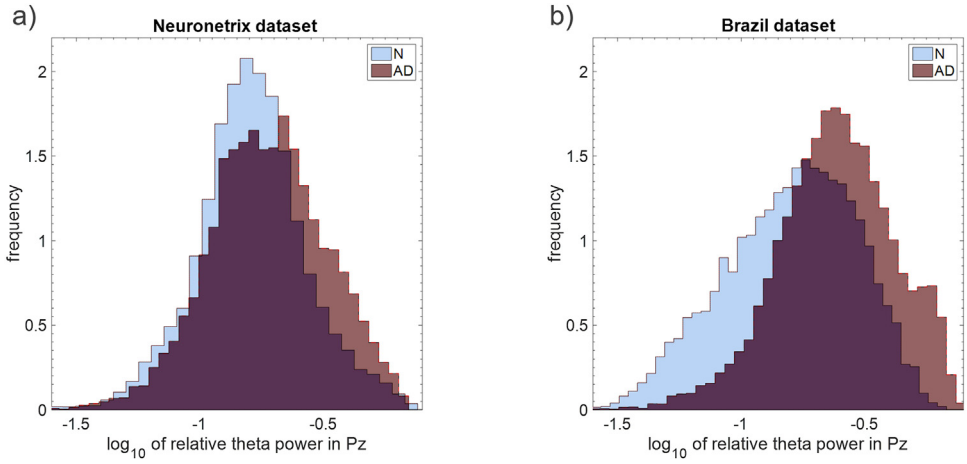

Fig. 8. Histograms for theta relative power in electrode Pz. (a) Neuronetrix and (b) Brazil dataset.

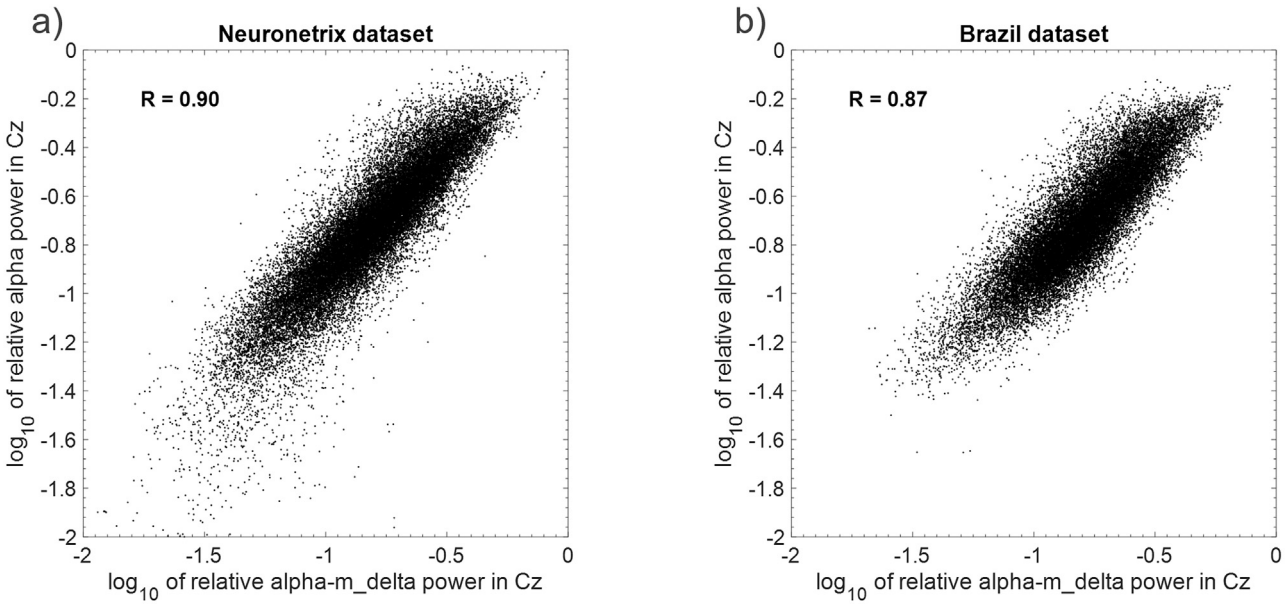

Fig. 9. Correlation between features alpha relative power and alpha-mdelta relative power for electrode Cz. (a) Neuronetrix and (b) Brazil dataset.

Table 7
Top-35 features across the different feature groups and frequency bands.

	Neuronetrix	Brazil
Spectral features	31	27
Coherence	4	5
Amplitude Modulation	0	3
Delta	4	3
Theta	3	5
Alpha	11	13
Beta	6	8
Gamma	6	6

in [48] and resting-awake eyes-closed-eyes in [49] and [50]. The same behaviour was observed in our results where power features in gamma band presented: (1) an increment in the Neuronetrix dataset (resting-awake eyes-open condition) and (2) a decrement in the Brazil dataset, (resting-awake eyes-closed condition), thus corroborating previous findings.

For both datasets, the top feature was alpha power for the electrode placed in Cz, which had a median value significantly lower in AD compared with the control cohort, as per Fig. 7. On the other hand, the opposite behaviour was observed in low frequency power features such as delta and theta. For example, the median of the theta power for the electrode Pz was significantly higher in AD cohort, as per Fig. 8.

While alpha power in Cz and theta power in Pz presented significant difference in both datasets, it is possible to appreciate (Figs. 7 and 8) that only one feature does not have sufficient classification power to accurately discriminate the AD and N groups, thus a combination of features is needed. Table 7 lists the distribution of the top-35 features across the different feature groups and frequency bands.

Interestingly, no amplitude modulation features appeared in the top-35 features in the Neuronetrix dataset. On the other hand, in the Brazil dataset all amplitude modulation features were high frequency bands (beta and gamma) modulated by alpha rhythm. While amplitude modulation features are corrupted by wICA [24], they provide information that is not present in spectral features, helping to a better classification. Another reason for the low number of amplitude modulation features in the top-35 is that features where a higher frequency band (alpha, beta or gamma) is modulated by a slow frequency (delta or theta) present a high correlation with the power features of the higher band. Fig. 9 shows the correlation between the power for alpha band in Cz (top feature in both datasets) and power of alpha_mdelta in Cz for Neuronetrix (Fig. 9a) and Brazil (Fig. 9b) dataset.

6. Conclusion

Here, a fully-automated, low-density (7 electrodes) EEG-based system for Alzheimer's disease detection has been proposed, tested, and validated. The wICA algorithm was utilized for automated artefact removal; from artefact-free signals, spectral, amplitude modulation and coherence features were computed to quantify the effects of AD on the EEG signals; later, the datasets were divided in Control (N) and AD by using a SVM-based classifier together with the LOSO CV in order to recreate realistic conditions. The proposed system was evaluated in two different datasets, namely Neuronetrix and Brazil, which consisted of resting state EEG data with open and closed eyes, respectively. Results show similarities between the two resting state protocols, specifically in most relevant features, even when the recording conditions were different. Similar analyses are still needed to assess the performance of such low-density layouts under different experimental protocols for AD diagnosis.

Conflict of interest statement

The authors declare that there is no conflict of interest regarding the publication of this paper.

Acknowledgements

This work was funded by the Natural Sciences and Engineering Research Council of Canada (NSERC) Discovery Grant RGPIN 402237-2011, the Start-up funding for INRS professors and the Foundation for Research Support of the State of São Paulo (FAPESP) Grant 2015/09510-7.

References

[1] WHO, and Alzheimer's Disease International. Dementia: A Public Health Priority. World Health Organization [Internet]. Available from: http://www.who.int/mental_health/publications/dementia_report_2012/en/ 2012 (Accessed 1 March 2016).
[2] Alzheimer's Disease Facts and Figures. Alzheimer's Association [Internet]. 2015. Available from https://www.alz.org/downloads/Facts_Figures_2015.pdf 2015 (Accessed 1 March 2016).
[3] Global Impact of Dementia 2013–2050. Alzheimer's Disease International [Internet]. Available from: http://www.alz.co.uk/research/G8-policy-brief 2013 (Accessed 1 March 2016).
[4] D. Galimberti, E. Scarpini, Disease-modifying treatments for Alzheimer's disease, Ther. Adv. Neurol. Disord. 4 (July (4)) (2011) 203–216, http://dx.doi.org/10.1177/1756285611404470.
[5] B. Dubois, H.H. Feldman, C. Jacova, S.T. DeKosky, P. Barberger-Gateau, J. Cummings, et al., Research criteria for the diagnosis of Alzheimer's disease: revising the NINCDS–ADRDA criteria, Lancet Neurol. 6 (August (8)) (2007) 734–746, http://dx.doi.org/10.1016/S1474-4422(07)70178-3.
[6] M. Sarazin, L.C. de Souza, S. Lehéricy, B. Dubois, Clinical and research diagnostic criteria for Alzheimer's disease, Neuroimaging Clin. North Am. 22 (February (1)) (2012) 23–32, http://dx.doi.org/10.1016/j.nic.2011.11.004.
[7] Barua B, Esmail N. Waiting your turn: wait times for health care in Canada, 2014 report. Fraser Institute, Studies in Health Policy [Internet]. Available from https://www.fraserinstitute.org/sites/default/files/waiting-your-turn-2014.pdf 2013 (Accessed 15 March 2016).
[8] P.L. Nunez, R. Srinivasan, Electric Fields of the Brain: The Neurophysics of EEG, Oxford University Press, Oxford; New York, 2006, ISBN: 0-19-505038-X 978-0-19-505038-7.
[9] J. Jeong, EEG dynamics in patients with Alzheimer's disease, Clin. Neurophysiol. 115 (July (7)) (2004) 1490–1505, http://dx.doi.org/10.1016/j.clinph.2004.01.001.
[10] J. Dauwels, F. Vialatte, A. Cichocki, Diagnosis of Alzheimer's disease from EEG signals: where are we standing? Curr. Alzheimer Res. 7 (September (6)) (2010) 487–505.
[11] K. Bennys, G. Rondouin, C. Vergnes, J. Touchon, Diagnostic value of quantitative EEG in Alzheimer's disease, Neurophysiol. Clin. Clin. Neurophysiol. 31 (June (3)) (2001) 153–160.
[12] T. Locatelli, M. Cursi, D. Liberati, M. Franceschi, G. Comi, EEG coherence in Alzheimer's disease, Electroencephalogr. Clin. Neurophysiol. 106 (March (3)) (1998) 229–237, http://dx.doi.org/10.1016/S0013-4694(97)00129-6.
[13] J. Dauwels, F. Vialatte, T. Musha, A. Cichocki, A comparative study of synchrony measures for the early diagnosis of Alzheimer's disease based on EEG, NeuroImage 49 (January (1)) (2010) 668–693, http://dx.doi.org/10.1016/j.neuroimage.2009.06.056.
[14] C. Babiloni, M. Pievani, F. Vecchio, C. Geroldi, F. Eusebi, C. Fracassi, et al., White-matter lesions along the cholinergic tracts are related to cortical sources of EEG rhythms in amnesic mild cognitive impairment, Hum. Brain Mapp. 30 (May (5)) (2009) 1431–1443, http://dx.doi.org/10.1002/hbm.20612.
[15] L.R. Trambaiolli, T.H. Falk, F.J. Fraga, R. Anghinah, A.C. Lorena, EEG spectro-temporal modulation energy: a new feature for automated diagnosis of Alzheimer's disease, 2011 Annual International Conference of the IEEE Engineering in Medicine and Biology Society, EMBC (2011), p. 3828–31.
[16] T.H. Falk, F.J. Fraga, L. Trambaiolli, R. Anghinah, EEG amplitude modulation analysis for semi-automated diagnosis of Alzheimer's disease, EURASIP J. Adv. Signal Process. 2012 (1) (2012) 1–9, http://dx.doi.org/10.1186/1687-6180-2012-192.
[17] F.J. Fraga, T.H. Falk, P.A.M. Kanda, R. Anghinah, Characterizing Alzheimer's disease severity via resting-awake EEG amplitude modulation analysis, PLoS One 8 (August (8)) (2013) e72240, http://dx.doi.org/10.1371/journal.pone.0072240, Ben-Jacob E. (Ed.).
[18] H. Adeli, S. Ghosh-Dastidar, N. Dadmehr, Alzheimer's disease: models of computation and analysis of EEGs, Clin. EEG Neurosci. 36 (3) (2005) 131–140, http://dx.doi.org/10.1177/155005940503600303.
[19] R. Cassani, T.H. Falk, F.J. Fraga, P.A.M. Kanda, R. Anghinah, The effects of automated artifact removal algorithms on electroencephalography-based Alzheimer's disease diagnosis, Front. Aging Neurosci. 6 (2014) 55, http://dx.doi.org/10.3389/fnagi.2014.00055.

[20] A.T. Reid, A.C. Evans, Structural networks in Alzheimer's disease, Eur. Neuropsychopharmacol. 23 (January (1)) (2013) 63–77, http://dx.doi.org/10.1016/j.euroneuro.2012.11.010.
[21] S.I. Dimitriadis, N.A. Laskaris, M.P. Bitzidou, I. Tarnanas, M.N. Tsolaki, A novel biomarker of amnestic MCI based on dynamic cross-frequency coupling patterns during cognitive brain responses, Front. Neurosci. 350 (2015), http://dx.doi.org/10.3389/fnins.2015.00350.
[22] J.M. Peters, T. Hummel, T. Kratzsch, J. Lötsch, C. Skarke, L. Frölich, olfactory function in mild cognitive impairment and Alzheimer's disease: an investigation using psychophysical and electrophysiological techniques, AJP 160 (November (11)) (2003) 1995–2002, http://dx.doi.org/10.1176/appi.ajp.160.11.1995.
[23] B. Güntekin, E. Saatçi, G. Yener, Decrease of evoked delta, theta and alpha coherences in Alzheimer patients during a visual oddball paradigm, Brain Res. 1235 (October) (2008) 109–116, http://dx.doi.org/10.1016/j.brainres.2008.06.028.
[24] D.A. Casey, Event-related potentials and the diagnosis of Alzheimer's disease—The COGNISIONTM System, US Neurol. 06 (02) (2010) 34, http://dx.doi.org/10.17925/USN.2010.06.02.34.
[25] R. Kurimoto, R. Ishii, L. Canuet, K. Ikezawa, M. Iwase, M. Azechi, et al., Induced oscillatory responses during the Sternberg's visual memory task in patients with Alzheimer's disease and mild cognitive impairment, NeuroImage. 59 (February (4)) (2012) 4132–4140, http://dx.doi.org/10.1016/j.neuroimage.2011.10.061.
[26] M. Karrasch, M. Laine, J.O. Rinne, P. Rapinoja, E. Sinervä, C.M. Krause, Brain oscillatory responses to an auditory-verbal working memory task in mild cognitive impairment and Alzheimer's disease, Int. J. Psychophysiol. 59 (February (2)) (2006) 168–178, http://dx.doi.org/10.1016/j.ijpsycho.2005.04.006.
[27] D.V. Moretti, A. Prestia, C. Fracassi, G. Binetti, O. Zanetti, G.B. Frisoni, Specific EEG changes associated with atrophy of hippocampus in subjects with mild cognitive impairment and Alzheimer's disease, Int. J. Alzheimer's Dis. 12 (February (2012)) (2012) e253153, http://dx.doi.org/10.1155/2012/253153.
[28] I. Daly, N. Nicolaou, S.J. Nasuto, K. Warwick, Automated artifact removal from the electroencephalogram: a comparative study, Clin. EEG Neurosci. 44 (October (4)) (2013) 291–306, http://dx.doi.org/10.1177/1550059413476485.
[29] J.A. Urigüen, B. Garcia-Zapirain, EEG artifact removalüstate-of-the-art and guidelines, J. Neural Eng. 12 (June (3)) (2015) 031001, http://dx.doi.org/10.1088/1741-2560/12/3/031001.
[30] T.P. Jung, S. Makeig, C. Humphries, T.W. Lee, M.J. McKeown, V. Iragui, et al., Removing electroencephalographic artifacts by blind source separation, Psychophysiology 37 (March (2)) (2000) 163–178, http://dx.doi.org/10.1111/1469-8986.3720163.
[31] A. Delorme, T. Sejnowski, S. Makeig, Enhanced detection of artifacts in EEG data using higher-order statistics and independent component analysis, Neuroimage 34 (February (4)) (2007) 1443–1449, http://dx.doi.org/10.1016/j.neuroimage.2006.11.004.
[32] D.P. He, G. Wilson, C. Russell, Removal of ocular artifacts from electro-encephalogram by adaptive filtering, Med. Biol. Eng. Comput. 42 (May (3)) (2004) 407–412, http://dx.doi.org/10.1007/BF02344717.
[33] N.P. Castellanos, V.A. Makarov, Recovering EEG brain signals: artifact suppression with wavelet enhanced independent component analysis, J. Neurosci. Methods 158 (December (2)) (2006) 300–312, http://dx.doi.org/10.1016/j.jneumeth.2006.05.033.
[34] F.J. Fraga, T.H. Falk, L.R. Trambaiolli, E.F. Oliveira, W.H.L. Pinaya, P.A.M. Kanda, et al., Towards an EEG-based biomarker for Alzheimer's disease: improving amplitude modulation analysis features, 2013 IEEE International Conference on Acoustics, Speech and Signal Processing (ICASSP) (2013) 1207–1211, http://dx.doi.org/10.1109/ICASSP.2013.6637842.
[35] J. Solé-Casals, F.-B. Vialatte, Towards semi-automatic artifact rejection for the improvement of Alzheimer's sisease screening from EEG signals, Sensors 15 (July (8)) (2015) 17963–17976, http://dx.doi.org/10.3390/s150817963.
[36] I. Genuth, All in the mind, Eng. Technol. 10 (June (5)) (2015) 37–39, http://dx.doi.org/10.1049/et.2015.0502.
[37] V. Mihajlović, B. Grundlehner, R. Vullers, J. Penders Wearable, Wireless EEG solutions in daily life applications: what are we missing? IEEE J. Biomed. Health Inf. 19 (January (1)) (2015) 6–21, http://dx.doi.org/10.1109/JBHI.2014.2328317.
[38] M. Cecchi, D.K. Moore, C.H. Sadowsky, P.R. Solomon, P.M. Doraiswamy, C.D. Smith, et al., A clinical trial to validate event-related potential markers of Alzheimer's disease in outpatient settings, Alzheimer's Dement. Diagn. Assess. Dis. Monit. 1 (4) (2015) 387–394, http://dx.doi.org/10.1016/j.dadm.2015.08.004.
[39] Guideline 6: A Proposal for Standard Montages to Be Used in Clinical EEG. American Clinical Neurophysiology Society [Internet]. 2006 (Accessed 27 March 2016) https://www.acns.org/pdf/guidelines/Guideline-6.pdf.
[40] G. Nolte, O. Bai, L. Wheaton, Z. Mari, S. Vorbach, M. Hallett, Identifying true brain interaction from EEG data using the imaginary part of coherency, Clin. Neurophysiol. 115 (October (10)) (2004) 2292–2307, http://dx.doi.org/10.1016/j.clinph.2004.04.029.
[41] C. Lehmann, T. Koenig, V. Jelic, L. Prichep, R.E. John, L.-O. Wahlund, et al., Application and comparison of classification algorithms for recognition of Alzheimer's disease in electrical brain activity (EEG), J. Neurosci. Methods 161 (April (2)) (2007) 342–350, http://dx.doi.org/10.1016/j.jneumeth.2006.10.023.
[42] C. Cortes, V. Vapnik, Support-vector networks, Mach. Learn. 20 (September (3)) (1995) 273–297, http://dx.doi.org/10.1007/BF00994018.
[43] A. Ben-Hur, J. Weston, A user's guide to support vector machines, in: O. Carugo, F. Eisenhaber (Eds.), Data Mining Techniques for the Life Sciences, Humana Press, 2010, pp. 223–239, http://dx.doi.org/10.1007/978-1-60327-241-4_13.
[44] J. Zhu, S. Rosset, T. Hastie, R. Tibshirani, 1-norm support vector machines, Adv. Neural Inf. Process. Syst. 16 (1) (2004) 49–56.
[45] F. Pedregosa, G. Varoquaux, A. Gramfort, V. Michel, B. Thirion, O. Grisel, et al., Scikit-Learn: Machine Learning in Python, J. Mach. Learn. Res., 2011, pp. 2825–2830, Nov 12, ISSN: 1532-4435.
[46] R. Cassani, T.H. Falk, F.J. Fraga, P.A. Kanda, R. Anghinah, Towards automated EEG-Based Alzheimer's disease diagnosis using relevance vector machines, 5th ISSNIP-IEEE Biosignals and Biorobotics Conference (2014): Biosignals and Robotics for Better and Safer Living (BRC) (2014) 1–6, http://dx.doi.org/10.1109/BRC.2014.6880978.
[47] H. Abdi, The Bonferonni and Šidák corrections for multiple comparisons, in: N.J. Salkind (Ed.), Encyclopedia of Measurement and Statistics, Sage Publications, 2006, pp. 103–107, ISBN: 9781412916110.
[48] J.A. Deursen, E.F.P.M. Vuurman, F.R.J. Verhey, V.H.J.M. Kranen-Mastenbroek, W.J. Riedel, Increased EEG gamma band activity in Alzheimer's disease and mild cognitive impairment, J. Neural Transm. 115 (July (9)) (2008) 1301–1311, http://dx.doi.org/10.1007/s00702-008-0083-y.
[49] D.V. Moretti, C. Fracassi, M. Pievani, C. Geroldi, G. Binetti, O. Zanetti, et al., Increase of theta/gamma ratio is associated with memory impairment, Clin. Neurophysiol. 120 (February (2)) (2009) 295–303, http://dx.doi.org/10.1016/j.clinph.2008.11.012.
[50] C.J. Stam, C.W. Van van, Y.A.L. Pijnenburg, H.W. Berendse, M. De, P. Scheltens, et al., Generalized synchronization of MEG recordings in Alzheimer's disease: evidence for involvement of the gamma band, J. Clin. Neurophysiol. 19 (6) (2002) 562–574, http://dx.doi.org/10.1097/00004691-200212000-00010.